

Nonergodic measurements of qubit frequency noise

Filip Wudarski,¹ Yaxing Zhang,² and M. I. Dykman³

¹USRA Research Institute for Advanced Computer Science (RIACS), Mountain View, CA 94043, USA

²Google Quantum AI, Santa Barbara, CA 93111, USA

³Department of Physics and Astronomy, Michigan State University, East Lansing, MI 48824, USA

Slow fluctuations of a qubit frequency are one of the major problems faced by quantum computers. To understand their origin it is necessary to go beyond the analysis of their spectra. We show that characteristic features of the fluctuations can be revealed using comparatively short sequences of periodically repeated Ramsey measurements, with the sequence duration smaller than needed for the noise to approach the ergodic limit. The outcomes distribution and its dependence on the sequence duration are sensitive to the nature of noise. The time needed for quantum measurements to display quasi-ergodic behavior can strongly depend on the measurement parameters.

I. INTRODUCTION

Due to the probabilistic nature of quantum measurements, many currently implemented quantum algorithms rely on repeatedly running a quantum computer. It is important that the qubit parameters remain essentially the same between the runs. This imposes a constraint on comparatively slow fluctuations of the qubit parameters, in particular qubit frequencies, and on developing means of revealing and characterizing such fluctuations.

Slow qubit frequency fluctuations have been a subject of intense studies [1–23]. Of primary interest has been their spectrum, although their statistics has also attracted interest [24–33]. This statistics is important as it may help to reveal the source of the underlying noise. In particular, fluctuations from the coupling to a few TLSs should be non-Gaussian [25, 30, 34–40]. The fluctuation statistics has been often described in terms of higher-order time correlators or their Fourier transforms, bi-spectra and high-order spectra. Most work thus far has been done on fluctuations induced by noise with the correlation time smaller than the qubit decay time.

Here we show that important information about qubit frequency fluctuations can be extracted from what we call nonergodic measurements. The idea is to perform M successive qubit measurements (for example, Ramsey measurements) over time longer than the qubit decay time but shorter than the noise correlation time. The measurement outcomes are determined by the instantaneous state of the noise source, for example, by the instantaneous TLSs' states. They vary from one series of M measurements to another. Thus the outcome distribution reflects the distribution of the noise source over its states. It provides information that is washed out in the ensemble averaging inherent to ergodic measurements.

Closely related is the question of how long should a quantum measurement sequence be to reach the ergodic limit in which the noise source explores all its states. Does the measurement duration depend on the type and parameters of the measurement, not only the noise source properties, and if so, on which parameters?

A convenient and frequently used method of performing successive measurements is to repeat them periodically.

In this case the duration of data acquisition of M measurements is $\propto M$. For the measurements to be nonergodic it should suffice for this duration to be smaller than the noise correlation time. This imposes a limitation on M from above. The limitation on M from below is imposed by the uncertainty that comes from the quantum nature of the measurements and thus requires statistical averaging over the outcomes.

We consider a periodic sequence of Ramsey measurements sketched in Fig. 1. At the beginning of a measurement the qubit, initially in the ground state $|0\rangle$, is rotated about the y -axis of the Bloch sphere by $\pi/2$, which brings it to the state $(|0\rangle + |1\rangle)/\sqrt{2}$. After time t_R the rotation is repeated and is followed by a projective measurement of finding the qubit in state $|1\rangle$. The qubit is then reset to $|0\rangle$, cf. [41]. In our scheme the measurements are repeated $M \gg 1$ times, with period t_{cyc} .

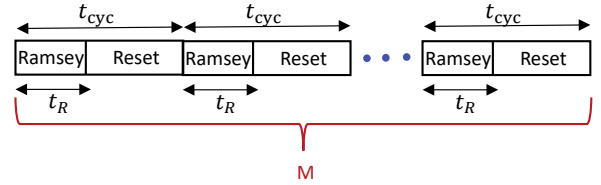


FIG. 1. Schematics of M Ramsey measurements. In each measurement the qubit phase is accumulated over time t_R . The measurements give the probability p to find the qubit in state $|1\rangle$. After a measurement the qubit is reset to state $|0\rangle$. The measurements are repeated with period t_{cyc} .

The outcome of a k th Ramsey measurement x_k is 0 or 1. The probability p to find $x_k = 1$ is determined by the qubit phase accumulated over time t_R . This phase comes from the detuning of the qubit frequency from the frequency of the reference drive and from the noise-induced qubit frequency fluctuations $\delta\omega_q(t)$. The detuning is controllable, and we will use ϕ_R to indicate the phase that comes from it. The Hamiltonian H_{fl} that describes frequency fluctuations and the phase θ_k accumulated in the k th measurement due to these fluctuations have the form

$$H_{\text{fl}} = -\frac{1}{2}\delta\omega_q(t)\sigma_z, \quad \theta_k = \int_{kt_{\text{cyc}}}^{kt_{\text{cyc}}+t_R} \delta\omega_q(t)dt. \quad (1)$$

Here we have set $\hbar = 1$; we associate the Pauli operators $\sigma_{x,y,z}$ with the operators acting on the qubit states. We are interested in slow frequency fluctuations. The correlation time of $\delta\omega_q(t)$ is $\gtrsim t_{\text{cyc}}$ and may significantly exceed the reciprocal qubit decay rate.

In terms of the phases θ and ϕ_R , the probability to have $x_k = 1$ is [42]

$$p(\theta) = \frac{1}{2} \left[1 + e^{-t_R/T_2} \cos(\phi_R + \theta) \right], \quad (2)$$

where T_2^{-1} is the qubit decoherence rate due to fast processes leading to decay and dephasing. In the absence of qubit frequency noise $\theta = 0$ for all M measurements and the distribution of the measurement outcomes is a binomial distribution [43]. Because of the frequency noise, the phase θ in Eq. (2) becomes random, changing from one measurement to another, and thus the probability $p(\theta)$ also becomes random. Then the outcomes distribution is determined not just by the quantum randomness, but also by the distribution of the values of θ .

The randomness of the phase is captured by the probability $\rho(m|M)$ to have $x_k = 1$ as a measurement outcome m times in M measurements, $\rho(m|M) = \text{Prob}(\sum_{k=1}^M x_k = m)$. We consider $\rho(m|M)$ for periodically repeated measurements, see Fig. 1. If the frequency noise has correlation time small compared to the period t_{cyc} , the phases θ_k in successive measurements are uncorrelated. Then $\rho(m|M)$ is still given by a binomial distribution,

$$\rho_{\text{binom}}(m|M) = \binom{M}{m} r_1^m (1 - r_1)^{M-m}, \quad (3)$$

where $r_1 \equiv \langle x_k \rangle = \langle p(\theta) \rangle_\theta$; here $\langle \dots \rangle_\theta$ indicates averaging over realizations of θ . For large M this distribution is close to a Gaussian peak centered at r_1 .

We are interested in the opposite case of slow frequency noise. Here the distribution $\rho(m|M)$ can strongly deviate from the binomial distribution. The deviation becomes pronounced and characteristic of the noise if Mt_{cyc} is comparable or smaller than the noise correlation time while M is still large.

The effect is particularly clear in the *static limit*, where the noise does not change over time Mt_{cyc} , i.e., the phase θ remains constant during M measurements. Even though θ is constant, its value $\theta = \theta(\ell)$ is random, it varies from one series of M measurements to another; here ℓ enumerates the series, and we assume that noise correlations decay between successive series. The probability $P[\theta(\ell)]$ to have a given $\theta(\ell)$ is determined by the noise statistics. The distribution of the outcomes $\rho(m|M)$ is obtained by averaging the results of multiply repeated series of M measurements. Extending the familiar arguments that lead to Eq. (3), we find

$$\begin{aligned} \rho(m|M) &= \binom{M}{m} \sum_{\ell} P[\theta(\ell)] p^m[\theta(\ell)] \\ &\times \{1 - p[\theta(\ell)]\}^{M-m} \end{aligned} \quad (4)$$

The distribution (4) directly reflects the distribution of the noise over its states. In particular, if the values of $\theta(\ell)$ are discrete and well-separated (see an example below), $\rho(m|M)$ has a characteristic fine structure with peaks located at $m \approx Mp[\theta(\ell)]$ for $M \gg 1$; the peak heights are determined by $P[\theta(\ell)]$.

An important example of slow frequency noise is the noise that results from dispersive coupling to a set of slowly switching TLSs,

$$\delta\omega_q(t) = \sum_n V^{(n)} \hat{\tau}_z^{(n)}. \quad (5)$$

Here $n = 1, \dots, N_{\text{TLS}}$ enumerates the TLSs, $\hat{\tau}_z^{(n)}$ is the Pauli operator of the n th TLS, and $V^{(n)}$ is the coupling parameter; the states of the n th TLS are $|0\rangle^{(n)}$ and $|1\rangle^{(n)}$, and $\hat{\tau}_z^{(n)} |i\rangle^{(n)} = (-1)^i |i\rangle^{(n)}$ with $i = 0, 1$. We assume that the TLSs do not interact with each other. Their dynamics is described by the balance equations for the state populations. The only parameters are the rates $W_{ij}^{(n)}$ of $|i\rangle^{(n)} \rightarrow |j\rangle^{(n)}$ transitions, where $i, j = 0, 1$ [44]. The rates $W_{ij}^{(n)}$ also give the stationary occupations of the TLSs states $w_{0,1}^{(n)}$,

$$w_0^{(n)} = W_{10}^{(n)} / W^{(n)}, \quad w_1^{(n)} = W_{01}^{(n)} / W^{(n)}. \quad (6)$$

Here $W^{(n)} = W_{01}^{(n)} + W_{10}^{(n)}$ is the TLS relaxation rate. The value of $\min W^{(n)}$ gives the reciprocal correlation time of the noise from the TLSs.

In the static-limit approximation, the TLSs remain in the initially occupied states $|0\rangle^{(n)}$ or $|1\rangle^{(n)}$ during all M measurements. Then, from Eq. (5), the phase $\delta\omega_q t_R$ that the qubit accumulates during a measurement is

$$\theta(\{j_n\}) = \sum_n V^{(n)} (-1)^{j_n} t_R, \quad (7)$$

where $j_n = 0$ if the occupied TLS state is $|0\rangle^{(n)}$ and $j_n = 1$ if the occupied state is $|1\rangle^{(n)}$. The probability to have a given $\theta(\{j_n\})$ is determined by the stationary state occupations, $P[\theta(\{j_n\})] = \prod_n w_{j_n}^{(n)}$.

For the TLSs' induced noise, ℓ in Eq. (4) enumerates various combinations $\{j_n\}$. With the increasing coupling $V^{(n)}$, the separation of the values of $\theta(\{j_n\})$ increases, helping to observe the fine structure of $\rho(m|M)$.

The expression for $\rho(m|M)$ simplifies in the important case where the TLSs are symmetric, $w_0^{(n)} = w_1^{(n)} = 1/2$, and all coupling parameters are the same, $V^{(n)} = V$, cf. [9, 45]. In this case $\theta(\{j_n\})$ takes on values $\theta_{\text{sym}}(\ell) = V t_R (2\ell - N_{\text{TLS}})$ with $0 \leq \ell \leq N_{\text{TLS}}$, and

$$\begin{aligned} \rho(m|M) &= 2^{-N_{\text{TLS}}} \binom{M}{m} \sum_{\ell} \binom{N_{\text{TLS}}}{\ell} p^m[\theta_{\text{sym}}(\ell)] \\ &\times \{1 - p[\theta_{\text{sym}}(\ell)]\}^{M-m}. \end{aligned} \quad (8)$$

The phases $\theta_{\text{sym}}(\ell)$ are determined by the coupling constant V multiplied by the difference of the number of

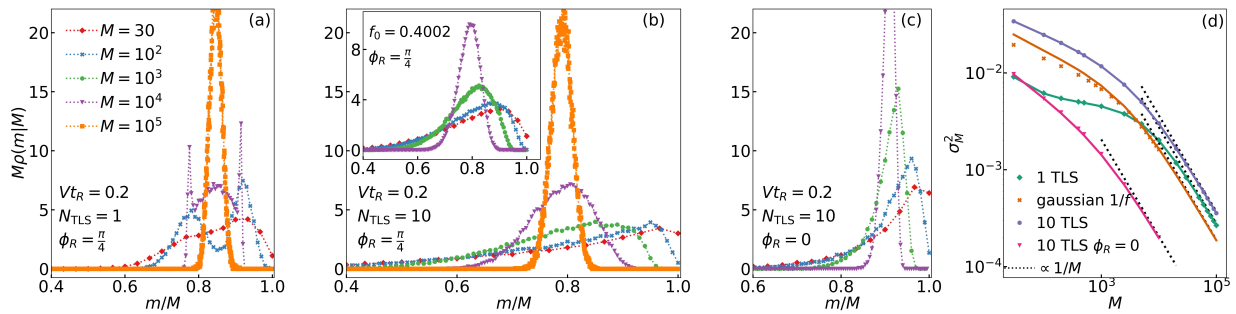


FIG. 2. Transition from nonergodic to ergodic behavior with the increasing number of measurements. Red diamonds, blue crosses, green dots, purple triangles, and orange squares in panels (a)-(c) show $\rho(m|M)$ for $M = 30, 10^2, 10^3, 10^4$ and 10^5 , respectively. The parameter of the dispersive qubit-to-TLS coupling is $Vt_R = 0.2$. The control parameter ϕ_R is $\pi/4$ in panels (a) and (b). (a) Coupling to a single symmetric TLS with the scaled switching rate $Wt_R = 1.2 \times 10^{-4}$. (b) Coupling to 10 symmetric TLSs with the switching rates $W^{(n)}t_R = \exp(-3n/4)$, $n = 3, 4, \dots, 12$. The inset shows the results for Gaussian $1/f$ -type noise described in the text, $f_0 = \langle \delta\omega_q^2 \rangle t_R^2$. (c) Coupling to the same 10 TLSs as in panel (b), but for $\phi_R = 0$. (d) The variance of $\rho(m|M)$ for the data in panels (a)-(c); the solid lines show the theory, Eq. (9), the data points show the results of the simulations. The dashed lines show the ergodic limit.

TLSs in the states $|0\rangle$ and $|1\rangle$, so that $\theta_{\text{sym}}(\ell)$ may be significantly larger than for a single TLS [46].

The probability $\rho(m|M)$ of having “1” m times in M measurements has a characteristic form also in the case of Gaussian frequency fluctuations if the fluctuations are slow, so that $\delta\omega_q(t)$ does not change over time Mt_{cyc} . An important example of slow noise is $1/f$ noise. In the static limit $\rho(m|M)$ is described by an extension of Eq. (4), which takes into account that θ takes on continuous values. Respectively, one has to change in Eq. (4) from the sum over ℓ to the integral over $\theta(\ell)$, with $P[\theta(\ell)]$ becoming the probability density. For Gaussian noise $P[\theta(\ell)] = (2\pi f_0)^{-1/2} \exp[-\theta^2(\ell)/2f_0]$, where $f_0 = \langle \delta\omega_q^2 \rangle t_R^2$ (we assume that $\langle \delta\omega_q \rangle = 0$). The distribution $\rho(m|M)$ does not have fine structure, it depends only on the noise intensity in the static limit.

The opposite of the static limit is the ergodic limit, where Mt_{cyc} is much larger than the noise correlation time and the noise has time to explore all states during the measurements. In this limit $\rho(m|M)$ as a function of m/M has a narrow peak at $r_1 = \langle m/M \rangle \equiv \sum_m (m/M)\rho(m|M)$, with $\langle [(m/M) - r_1]^n \rangle \propto M^{1-n}$.

Simulations. We performed numerical simulations to explore the transition from the static to the ergodic limit and the features of $\rho(m|M)$ for slow noise. We used $t_{\text{cyc}} = 3t_R$. The measurements were simulated at least 10^5 times. In Figs. 2 and 3 we show $\rho(m|M)$ for the noise from symmetric TLSs, $W_{01}^{(n)} = W_{10}^{(n)} = W^{(n)}/2$. The results for asymmetric TLSs are similar [46].

Figure 2 shows evolution of $\rho(m|M)$ with the varying measurements number M . It is very different for different numbers of TLSs and the measurement parameter ϕ_R . The figure refers to a relatively weak qubit-TLS coupling. Panel (a) refers to a single TLS. Here, in the static limit $\rho(m|M)$ is double-peaked, with the peaks at $m/M \approx 0.92$ and 0.78 , from Eq. (8). Such peaks are seen for $M = 100$ and $M = 10^4$, where $MWt_{\text{cyc}} = 3.6 \times 10^{-2}$ and 3.6 , respectively, even though one might expect the

system to be close to ergodic for $M = 10^4$. For $M = 30$ the fine structure is smeared, because M is not large enough to average out the uncertainty of quantum measurements, but $\rho(m|M)$ displays a significant and characteristic asymmetry. For $M = 10^5$, where $MWt_{\text{cyc}} = 36$, the distribution does approach the ergodic limit, with a single peak at $m/M \approx 0.85$ [46].

Figure 2 (b) refers to 10 TLSs. Their scaled switching rates $W^{(n)}t_{\text{cyc}}$ form a geometric series, varying from ≈ 0.32 to $\approx 3.7 \times 10^{-4}$, so that the static limit does not apply and the fine structure is not resolved [46]. The asymmetry of $\rho(m|M)$ is profound. It gradually decreases with the increasing M . It is important that, for $\phi_R = \pi/4$, the distribution approaches the ergodic limit for $Mt_{\text{cyc}} \times (\min W^{(n)}) \gtrsim 30$, similar to the case of one TLS (the choice $\phi_R = \pi/4$ is explained in [46]).

The inset in Fig. 2 (b) shows the evolution of $\rho(m|M)$ for $1/f$ -type Gaussian frequency noise $\delta\omega_q(t)$ with the power spectrum $S_q(\omega) = (2D/\pi) \int_{\omega_{\text{min}}}^{\infty} dW/(W^2 + \omega^2)$. The cutoff frequency ω_{min} is set equal to the minimal switching rate of the 10 TLS in the main panel $\min(W^{(n)})$, and the intensity D is chosen so that, in the ergodic limit, $\rho(m|M)$ has a maximum for the same m/M as for the 10 TLSs [46]). Yet the evolution of $\rho(m|M)$ with the increasing M is fairly different from that in the main panel.

The result of Fig. 2 (c) is surprising. The data refers to the same 10 TLS as in panel (b), except that the phase of the Ramsey measurement is set to $\phi_R = 0$. The change of ϕ_R does not affect the dynamics of the TLSs. However, for the same M values, the peak of $\rho(m|M)$ is much narrower than where $\phi_R = \pi/4$ and the ergodic limit is approached by the measurement outcomes for an order of magnitude smaller M .

A simple measure of closeness of $\rho(m|M)$ to the ergodic limit is the variance $\sigma_M^2 = \sum_m (m/M)^2 \rho(m|M) - r_1^2$, where $r_1 = \langle x_k \rangle \equiv \sum_m (m/M)\rho(m|M)_{M \rightarrow \infty}$. A straight-

forward calculation shows that

$$\sigma_M^2 = M^{-1}r_1(1-r_1) + 2M^{-1} \sum_{k=1}^{M-1} \tilde{r}_2(k)[1 - (k/M)],$$

$$\tilde{r}_2(k) = \langle x_n x_{n+k} \rangle - \langle x_n \rangle^2 \quad (9)$$

($\tilde{r}_2(k)$ is the centered correlator of the measurement outcomes). For correlated noise $\rho(m|M)$ differs from the binomial distribution (3) and σ_M^2 is larger than its value $r_1(1-r_1)/M$ for uncorrelated noise. Still, in agreement with statistical physics, in the ergodic limit $\sigma_M^2 \propto M^{-1}$. In contrast, the static-limit value of σ_M^2 is generally much larger and scales differently with M .

Figure 2 (d) shows how σ_M^2 approaches the ergodic scaling. For $\phi_R = \pi/4$ and the same correlation time of the noise from 1 or 10 TLSs and of Gaussian noise ($\sim 1/\min W^{(n)}$ and $\sim 1/\omega_{\min}$), σ_M^2 behaves similarly for large M . Yet, for the same 10 TLSs, but for $\phi_R = 0$ the variance approaches the ergodic limit much faster.

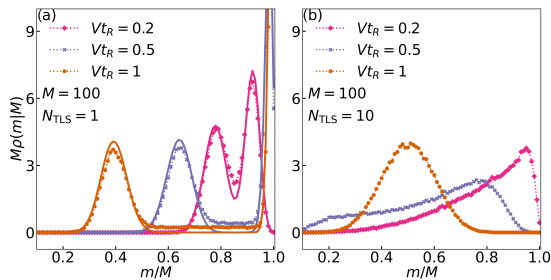


FIG. 3. Nonergodic behavior for a different strength of the qubit to TLSs coupling. The results refer to $M = 100$. (a) Coupling to a single TLS, $Wt_R = 10^3$. Solid lines show the static limit, Eq. (8). (b) Coupling to 10 TLSs with the same switching rates as in Fig. 2.

Figure 3 shows the effect of the strength of the coupling to the TLSs for an intermediate number of measurements $M = 100$. Panel (a) shows a profoundly double-peaked distribution for a single TLS, in excellent agreement with the static-limit (8). As expected, the distance between the peaks increases with the increasing coupling. For 10 TLSs, as seen in panel (b), the distribution is broad and strongly asymmetric. Both its shape and the position of the maximum sensitively depend on the coupling. It is important that the coupling parameter Vt_R can be changed in the experiment by varying t_R , which helps pointing to the mechanism of the noise. We note the

distinction from direct measurements of qubit frequency as a function of time [2, 5, 20], which is efficient for still much slower noise.

Discussion. To reach ergodic limit, a system of 10 TLSs has to visit its 2^{10} states. The needed time is a property of the TLSs themselves. However, the results of the measurements can approach quasi-ergodic limit, except for the far tail of the outcomes distribution, over a shorter time. This time depends on how the measurements are done. In our setup, the noise is measured by the qubit, and then the results are read through Ramsey measurements. An important parameter is the qubit-to-TLSs coupling, which we chose to be the same for all TLSs to avoid any bias. Unexpectedly, there is another important parameter, the phase ϕ_R .

The effect of ϕ_R on the convergence to the ergodic limit is not obvious in advance. It comes through the dependence on ϕ_R of the centered correlator $\tilde{r}_2(k)$ of the measurement outcomes. For weak coupling to slowly switching TLSs, $V^{(n)}t_R \ll 1$ and $W^{(n)}t_R \ll 1$, and for small ϕ_R this correlator is small. Moreover, it falls off with the increasing k much faster than for $\phi_R = \mathcal{O}(1)$ [46]. This indicates a reduced role of the noise correlations for small ϕ_R . Respectively, the ergodic limit is reached must faster with the increasing M .

Conclusions We studied the distribution of the outcomes of periodically repeated Ramsey measurements with the sequence length Mt_{cyc} shorter than needed to approach the ergodic limit. Such distribution proves to provide an alternative, and sensitive, means of characterizing qubit frequency noise with a long correlation time. The analytical results and simulations show that, for non-Gaussian noise, in particular the noise from TLSs, the distribution can display a characteristic fine structure. Even where there is no fine structure, the form of the distribution and its evolution with the sequence length are noise-specific.

The results show that the way the system approaches the ergodic limit with the increasing number of quantum measurements depends not only on the noise source, but also on the character and parameters of the measurement. These parameters are not necessarily known in advance. Their effect can be strong and depends on the noise source. Measurement outcomes can practically approach the ergodic limit well before the noise source approaches this limit.

FW and MID acknowledge partial support from NASA Academic Mission Services, Contract No. NNA16BD14C, and from Google under NASA-Google SAA2-403512.

- [1] Y. Nakamura, Yu. A. Pashkin, T. Yamamoto, and J. S. Tsai, Charge Echo in a Cooper-Pair Box, *Phys. Rev. Lett.* **88**, 047901 (2002).
 [2] R. C. Bialczak, R. McDermott, M. Ansmann, M. Hofheinz, N. Katz, E. Lucero, M. Neeley, A. D.

- O'Connell, H. Wang, A. N. Cleland, and J. M. Martinis, 1/f Flux Noise in Josephson Phase Qubits, *Phys. Rev. Lett.* **99**, 187006 (2007).
 [3] G. A. Álvarez and D. Suter, Measuring the Spectrum of Colored Noise by Dynamical Decoupling, *Phys. Rev.*

- Lett.* **107**, 230501 (2011).
- [4] J. Bylander, S. Gustavsson, F. Yan, F. Yoshihara, K. Harrabi, G. Fitch, D. G. Cory, Y. Nakamura, J.-S. Tsai, and W. D. Oliver, Noise spectroscopy through dynamical decoupling with a superconducting flux qubit, *Nat. Phys.* **7**, 565 (2011).
- [5] D. Sank, R. Barends, R. C. Bialczak, Y. Chen, J. Kelly, M. Lenander, E. Lucero, M. Mariantoni, A. Megrant, M. Neeley, P. J. J. O'Malley, A. Vainsencher, H. Wang, J. Wenner, T. C. White, T. Yamamoto, Y. Yin, A. N. Cleland, and J. M. Martinis, Flux Noise Probed with Real Time Qubit Tomography in a Josephson Phase Qubit, *Phys. Rev. Lett.* **109**, 067001 (2012).
- [6] F. Yan, J. Bylander, S. Gustavsson, F. Yoshihara, K. Harrabi, D. G. Cory, T. P. Orlando, Y. Nakamura, J.-S. Tsai, and W. D. Oliver, Spectroscopy of low-frequency noise and its temperature dependence in a superconducting qubit, *Phys. Rev. B* **85**, 174521 (2012).
- [7] K. C. Young and K. B. Whaley, Qubits as spectrometers of dephasing noise, *Phys. Rev. A* **86**, 012314 (2012).
- [8] G. A. Paz-Silva and L. Viola, General Transfer-Function Approach to Noise Filtering in Open-Loop Quantum Control, *Phys. Rev. Lett.* **113**, 250501 (2014).
- [9] F. Yoshihara, Y. Nakamura, F. Yan, S. Gustavsson, J. Bylander, W. D. Oliver, and J.-S. Tsai, Flux qubit noise spectroscopy using Rabi oscillations under strong driving conditions, *Phys. Rev. B* **89**, 020503 (2014).
- [10] M. Kim, H. J. Mamin, M. H. Sherwood, K. Ohno, D. D. Awschalom, and D. Rugar, Decoherence of Near-Surface Nitrogen-Vacancy Centers Due to Electric Field Noise, *Phys. Rev. Lett.* **115**, 087602 (2015).
- [11] M. Brownnutt, M. Kumph, P. Rabl, and R. Blatt, Ion-trap measurements of electric-field noise near surfaces, *Rev. Mod. Phys.* **87**, 1419 (2015).
- [12] P. J. J. O'Malley, J. Kelly, R. Barends, B. Campbell, Y. Chen, Z. Chen, B. Chiaro, A. Dunsworth, A. G. Fowler, I.-C. Hoi, E. Jeffrey, A. Megrant, J. Mutus, C. Neill, C. Quintana, P. Roushan, D. Sank, A. Vainsencher, J. Wenner, T. C. White, A. N. Korotkov, A. N. Cleland, and J. M. Martinis, Qubit Metrology of Ultralow Phase Noise Using Randomized Benchmarking, *Phys. Rev. Applied* **3**, 044009 (2015).
- [13] F. Yan, S. Gustavsson, A. Kamal, J. Birenbaum, A. P. Sears, D. Hover, T. J. Gudmundsen, D. Rosenberg, G. Samach, S. Weber, J. L. Yoder, T. P. Orlando, J. Clarke, A. J. Kerman, and W. D. Oliver, The flux qubit revisited to enhance coherence and reproducibility, *Nat Commun* **7**, 1 (2016).
- [14] B. A. Myers, A. Ariyaratne, and A. C. B. Jayich, Double-Quantum Spin-Relaxation Limits to Coherence of Near-Surface Nitrogen-Vacancy Centers, *Phys. Rev. Lett.* **118**, 197201 (2017).
- [15] C. M. Quintana, Y. Chen, D. Sank, A. G. Petukhov, T. C. White, D. Kafri, B. Chiaro, A. Megrant, R. Barends, B. Campbell, Z. Chen, A. Dunsworth, A. G. Fowler, R. Graff, E. Jeffrey, J. Kelly, E. Lucero, J. Y. Mutus, M. Neeley, C. Neill, P. J. J. O'Malley, P. Roushan, A. Shabani, V. N. Smelyanskiy, A. Vainsencher, J. Wenner, H. Neven, and J. M. Martinis, Observation of Classical-Quantum Crossover of $1/f$ Flux Noise and Its Paramagnetic Temperature Dependence, *Phys. Rev. Lett.* **118**, 057702 (2017).
- [16] G. A. Paz-Silva, L. M. Norris, and L. Viola, Multiqubit spectroscopy of Gaussian quantum noise, *Phys. Rev. A* **95**, 022121 (2017).
- [17] C. Ferrie, C. Granade, G. Paz-Silva, and H. M. Wiseman, Bayesian quantum noise spectroscopy, *New J. Phys.* **20**, 123005 (2018).
- [18] C. Noel, M. Berlin-Udi, C. Matthiesen, J. Yu, Y. Zhou, V. Lordi, and H. Häffner, Electric-field noise from thermally activated fluctuators in a surface ion trap, *Phys. Rev. A* **99**, 063427 (2019).
- [19] U. von Lüpke, F. Beaudoin, L. M. Norris, Y. Sung, R. Winik, J. Y. Qiu, M. Kjaergaard, D. Kim, J. Yoder, S. Gustavsson, L. Viola, and W. D. Oliver, Two-Qubit Spectroscopy of Spatiotemporally Correlated Quantum Noise in Superconducting Qubits, *PRX Quantum* **1**, 010305 (2020).
- [20] T. Proctor, M. Revelle, E. Nielsen, K. Rudinger, D. Lobser, P. Maunz, R. Blume-Kohout, and K. Young, Detecting and tracking drift in quantum information processors, *Nat Commun* **11**, 5396 (2020).
- [21] G. Wolfowicz, F. J. Heremans, C. P. Anderson, S. Kanai, H. Seo, A. Gali, G. Galli, and D. D. Awschalom, Qubit guidelines for solid-state spin defects, *Nat. Rev. Mater.* **6**, 906 (2021), comment: 40 pages, 7 figures, 259 references.
- [22] Y.-X. Wang and A. A. Clerk, Intrinsic and induced quantum quenches for enhancing qubit-based quantum noise spectroscopy, *Nat Commun* **12**, 6528 (2021).
- [23] S. Burgardt, S. B. Jäger, J. Feß, S. Hiebel, I. Schneider, and A. Widera, *Measuring the environment of a Cs qubit with dynamical decoupling sequences* (2023), [arXiv:2303.06983](https://arxiv.org/abs/2303.06983).
- [24] F. Li, A. Saxena, D. Smith, and N. A. Sinitsyn, Higher-order spin noise statistics, *New J. Phys.* **15**, 113038 (2013).
- [25] G. Ramon, Non-Gaussian signatures and collective effects in charge noise affecting a dynamically decoupled qubit, *Phys. Rev. B* **92**, 155422 (2015).
- [26] L. M. Norris, G. A. Paz-Silva, and L. Viola, Qubit Noise Spectroscopy for Non-Gaussian Dephasing Environments, *Phys. Rev. Lett.* **116**, 150503 (2016).
- [27] N. A. Sinitsyn and Y. V. Pershin, The theory of spin noise spectroscopy: A review, *Rep. Prog. Phys.* **79**, 106501 (2016).
- [28] P. Szańkowski, G. Ramon, J. Krzywda, D. Kwiatkowski, and L. Cywiński, Environmental noise spectroscopy with qubits subjected to dynamical decoupling, *J. Phys.: Condens. Matter* **29**, 333001 (2017).
- [29] Y. Sung, F. Beaudoin, L. M. Norris, F. Yan, D. K. Kim, J. Y. Qiu, U. von Lüpke, J. L. Yoder, T. P. Orlando, S. Gustavsson, L. Viola, and W. D. Oliver, Non-Gaussian noise spectroscopy with a superconducting qubit sensor, *Nat. Commun.* **10**, 3715 (2019).
- [30] G. Ramon, Trispectrum reconstruction of non-Gaussian noise, *Phys. Rev. B* **100**, 161302(R) (2019).
- [31] F. Sakuldee and L. Cywiński, Relationship between subjecting the qubit to dynamical decoupling and to a sequence of projective measurements, *Phys. Rev. A* **101**, 042329 (2020).
- [32] Y.-X. Wang and A. A. Clerk, Spectral characterization of non-Gaussian quantum noise: Keldysh approach and application to photon shot noise, *Phys. Rev. Res.* **2**, 033196 (2020).
- [33] X. You, A. A. Clerk, and J. Koch, Positive- and negative-frequency noise from an ensemble of two-level fluctuators, *Phys Rev Res.* **3**, 013045 (2021), [arxiv:2005.03591](https://arxiv.org/abs/2005.03591).
- [34] E. Paladino, L. Faoro, G. Falci, and R. Fazio, Decoher-

- ence and $1/f$ Noise in Josephson Qubits, *Phys. Rev. Lett.* **88**, 228304 (2002).
- [35] Y. M. Galperin, B. L. Altshuler, and D. V. Shantsev, Low-frequency noise as a source of dephasing of a qubit, in *Fundamental Problems of Mesoscopic Physics*, edited by I. V. Lerner (Kluwer Academic Publishing, The Netherlands, 2004) pp. 141–165, comment: 18 pages, 8 figures, Proc. of NATO/Euresco Conf. "Fundamental Problems of Mesoscopic Physics: Interactions and Decoherence", Granada, Spain, Sept.2003.
- [36] L. Faoro and L. Viola, Dynamical Suppression of $1/f$ Noise Processes in Qubit Systems, *Phys. Rev. Lett.* **92**, 117905 (2004).
- [37] Y. M. Galperin, B. L. Altshuler, J. Bergli, and D. V. Shantsev, Non-Gaussian Low-Frequency Noise as a Source of Qubit Decoherence, *Phys. Rev. Lett.* **96**, 097009 (2006).
- [38] E. Paladino, Y. M. Galperin, G. Falci, and B. L. Altshuler, $1/f$ noise: Implications for solid-state quantum information, *Rev. Mod. Phys.* **86**, 361 (2014).
- [39] C. Müller, J. H. Cole, and J. Lisenfeld, Towards understanding two-level-systems in amorphous solids: Insights from quantum circuits, *Rep. Prog. Phys.* **82**, 124501 (2019).
- [40] Z. Huang, X. You, U. Alyanak, A. Romanenko, A. Grassellino, and S. Zhu, [High-Order Qubit Dephasing at Sweet Spots by Non-Gaussian Fluctuators: Symmetry Breaking and Floquet Protection](#) (2022), [arxiv:2206.02827 \[quant-ph\]](#).
- [41] T. Fink and H. Bluhm, Noise Spectroscopy Using Correlations of Single-Shot Qubit Readout, *Phys. Rev. Lett.* **110**, 010403 (2013).
- [42] M. A. Nielsen and I. L. Chuang, *Quantum Computation and Quantum Information: 10th Anniversary Edition*, 1st ed. (Cambridge University Press, Cambridge ; New York, 2011).
- [43] N. G. Van Kampen, *Stochastic Processes in Physics and Chemistry*, 3rd ed. (Elsevier, Amsterdam, 2007).
- [44] P. W. Anderson, B. I. Halperin, and C. M. Varma, Anomalous low-temperature thermal properties of glasses and spin glasses, *Philos. Mag. J. Theor. Exp. Appl. Phys.* **25**, 1 (1972); W. A. Phillips, Tunneling states in amorphous solids, *J Low Temp Phys* **7**, 351 (1972); Two-Level States in Glasses, *Rep. Prog. Phys.* **50**, 1657 (1987).
- [45] G. Ithier, E. Collin, P. Joyez, P. J. Meeson, D. Vion, D. Esteve, F. Chiarello, A. Shnirman, Y. Makhlin, J. Schrieffer, and G. Schön, Decoherence in a superconducting quantum bit circuit, *Phys. Rev. B* **72**, 134519 (2005).
- [46] See Supplemental Material for more results on $\rho(m|M)$, including the fine structure, the effect of asymmetric TLSs, and the transition to the ergodic limit.

Supplemental materials: Nonergodic measurements of qubit frequency noise

Filip Wudarski

USRA Research Institute for Advanced Computer Science (RIACS), Mountain View, CA 94043, USA

Yaxing Zhang

Google Quantum AI, Santa Barbara, CA 93111, USA

M. I. Dykman

Department of Physics and Astronomy, Michigan State University, East Lansing, MI 48824, USA

I. COUPLING TO ASYMMETRIC TWO-LEVEL SYSTEMS

Generally, the switching rates W_{ij} between the states $|i\rangle$ and $|j\rangle$ of a two-level system (TLS) are different. TLSs with $W_{ij} \neq W_{ji}$ are called asymmetric. Here we present the results that show the effect of the TLS asymmetry on the qubit frequency noise for slow TLSs, where the rates W_{ij} are much smaller than the reciprocal duration of the Ramsey measurement. We consider a sequence of measurements described in the main text, where Ramsey measurements are periodically repeated M times with period t_{cyc} , see Fig. 1 of the main text.

Figure 1 shows the probability distribution $\rho(m|M)$ to have m “ones” in a sequence of M Ramsey measurements of duration t_R , which are periodically repeated with period $t_{\text{cyc}} = 3t_R$. A characteristic feature of the distribution for the coupling to slow TLSs is the possibility to have a fine structure. The fine structure can be approximately described in the static limit, where we disregard switching between the TLS states during the time Mt_{cyc} . As seen from Eq. (4) of the main text, for the coupling to a single TLS with states $|0\rangle$ and $|1\rangle$,

$$\rho(m|M) = \binom{M}{m} \sum_{\ell=0,1} P[\theta(\ell)] p^m [\theta(\ell)] \{1 - p[\theta(\ell)]\}^{M-m},$$

$$\theta(\ell) = (-1)^\ell V t_R, \quad P[(\theta(\ell))] = W_{1-\ell\ell}/W \quad (1)$$

where $W = W_{01} + W_{10}$ is the relaxation rate of the TLS and $p(\theta) = [1 + \cos(\theta + \phi_R)]/2$ is the probability of having “one” as a measurement outcome in the neglect of decoherence due to fast processes; $\theta = \int_0^{t_R} dt \delta\omega_q(t)$ is the qubit phase accumulated during Ramsey measurement due to qubit frequency fluctuations $\delta\omega_q(t)$; ϕ_R is the controlled qubit phase, see the main text.

For $M \gg 1$ the distribution (1) has two peaks, which are located at $m/M = p[\theta(\ell)]$ and have intensities $\propto W_{1-\ell\ell}/W$ ($\ell = 0, 1$). Such peaks are seen in panels (a) and (b) of Fig. 1 for $M = 100$, where $Mt_{\text{cyc}} \ll 1/W_{01}, 1/W_{10}$. The distance between the peaks is $\approx 2Vt_R$. For small M the structure is smeared by the uncertainty of quantum measurements. For large M , where $Mt_{\text{cyc}} \gg 1/W_{01}, 1/W_{10}$, the system approaches ergodic limit, where the TLS has time to explore its states over the duration Mt_{cyc} of the sequence of measurement.

Note a peculiar double-peak shape of the distribution for $M = 10^3$ in panel (a); it refers to the parameter values where $MW_{10}t_{\text{cyc}} > 1$ and $MW_{01}t_{\text{cyc}} < 1$, so that the has time to switch from state $|1\rangle$, but the probability to switch from state $|0\rangle$ is still relatively small. Such structure of $\rho(m|M)$ is a feature of asymmetric TLSs.

In the case of 10 TLSs with the parameters used in Fig. 1 the fine structure of $\rho(m|M)$ is not seen, similar to the case of symmetric TLSs presented in the main text, and for the same reason: $Mt_{\text{cyc}}W^{(n)} > 1$ for several TLSs once M becomes sufficiently large, $M \gtrsim 10^2$ (we recall that M has to be large to overcome the uncertainty of the outcomes of quantum measurements). The peaks of the distribution $\rho(m|M)$ are profoundly asymmetric. Their shape displays a characteristic change with the duration of the measurement sequence Mt_{cyc} and with the effective coupling strength controlled by the Ramsey measurement duration t_R .

The right panel of Fig. 2 shows how the variance of the distribution $\rho(m|M)$ approaches the ergodic limit $M \rightarrow \infty$ for the same system of 10 asymmetric TLSs as in Fig. 1 (c). As in the case of symmetric TLSs discussed in the main text and also in Sec. III, the variance strongly depends on the measurement phase ϕ_R . It is much smaller for $\phi_R = 0$ than for $\phi_R = \pi/4$. We explain in Sec. III that this is directly related to the behavior of the pair correlator $\tilde{r}_2(k)$, which is shown in the left panel of Fig. 2.

II. FINE STRUCTURE OF THE DISTRIBUTION FOR THE COUPLING TO MULTIPLE SYMMETRIC TLSS

As indicated in the main text, the fine structure can become more pronounced for several TLSs than for one TLS, provided their coupling to the qubit is the same and their switching rates are small. Figure 3 illustrates this effect for the coupling to five symmetric TLSs. The considered system is the five slower-switching TLSs studied in the main text, see Fig. 2 of the main text. In the static limit the qubit phase θ can take on 6 values, $\pm Vt_R, \pm 3Vt_R$, and $\pm 5Vt_R$, cf. Eq. (8) of the main text. However, the theory lines in Fig. 3 show 5 or 4 peaks, depending on the value of Vt_R . This is because the probability to have “one” as a measurement outcome is deter-

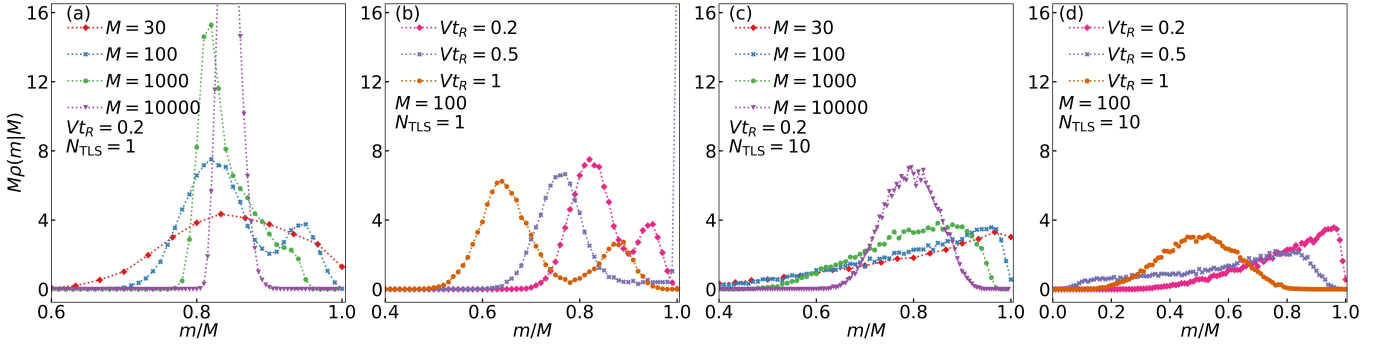


FIG. 1. Evolution of the probability distribution $\rho(m|M)$ for coupling to asymmetric TLSs. The measurement phase is $\phi_R = \pi/4$. The number of Ramsey measurements in a sequence M and the coupling parameters are indicated in the legends. The period at which the measurements are repeated within a sequence is $t_{\text{cyc}} = 3t_R$. Panels (a) and (b) refer to one TLS with the switching rates scaled by the duration t_R of the measurement being $W_{10t_R} = 0.00075$, $W_{01t_R} = 0.00025$. Panels (c) and (d) refer to 10 TLSs with the switching rates $W_{10t_R} = \exp(-3/4n)/2$, $W_{01t_R} = \exp(-3/4(n+1))/2$, where $n = 3, 4, \dots, 12$.

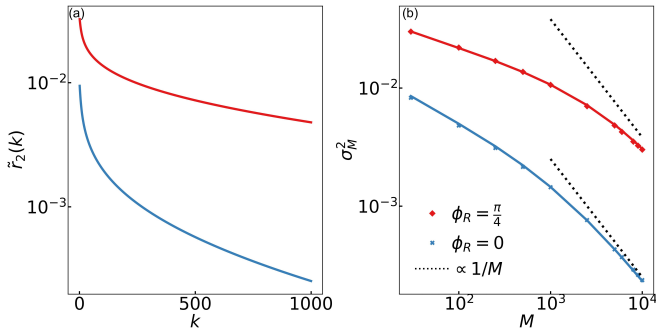


FIG. 2. Approaching the ergodic limit in the case of noise from asymmetric TLSs. The figure refers to 10 TLSs with the same coupling parameter and the same switching rates as in Fig. 1 (c). Left panel: calculated centered correlator $\tilde{r}_2(k)$ of the outcomes of qubit measurements, see Eqs. (2) and (3), for $\phi_R = \pi/4$ (red line) and $\phi_R = 0$ (blue line). Right panel: calculated (solid lines) and simulated (dots) variance $\sigma_M^2 = \sum_m (m/M)^2 \rho(m|M) - r_1^2$ of the distribution of the measurement outcomes. The dashed lines show the values of σ_M^2 in the ergodic limit where $\sigma_M^2 \propto 1/M$.

mined by $\cos(\theta + \phi_R)$. We use $\phi_R = \pi/4$, and some peaks appear to be too small to be resolved.

The value of $\phi_R = \pi/4$ is, in some sense, “generic”. The measurement outcomes could be expected to be more sensitive to noise for $\phi_R = \pi/2$. In particular, observing the fine structure of the distribution $\rho(m|M)$ is easier for $\phi_R = \pi/2$, as seen from Eqs. (4) - (8) of the main text. However, some correlators of the measurement outcomes can become zero for $\phi_R = \pi/2$, depending on the noise origin, and can be small for $\phi_R = 0$ [1]. This makes studying $\rho(m|M)$ for $\phi_R = \pi/4$ advantageous.

Overall, for $M = 100$ the static-limit theory is in a reasonably good agreement with the simulations. The numerical values of the parameter $W^{(n)}t_{\text{cyc}}$ form a geometric series and lie between $\approx 7.4 \times 10^{-3}$ and $\approx 3.7 \times 10^{-4}$. For $M = 100$ the condition $MW^{(n)}t_{\text{cyc}} \ll 1$ applies to most of the TLSs, and this is where the fine structure

is most pronounced. Interestingly, for $Vt_R = 1$ the fine structure is visible even for $M = 30$, where the distribution $\rho(m|M)$ is broadened by the uncertainty of the measurement outcomes. For $M = 10^3$ the distribution has a single broad peak for the both values of Vt_R . For still larger M the peak narrows down, so that ultimately the distribution approaches the ergodic limit.

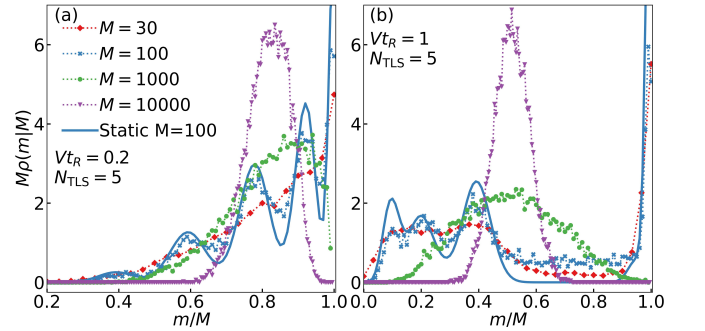


FIG. 3. Evolution of the probability distribution $\rho(m|M)$ with the increasing M for five symmetric TLSs, $W_{ij}^{(n)} = W_{ji}^{(n)} = W^{(n)}/2$. The coupling is the same for all TLSs and $\phi_R = \pi/4$. The switching rates are $W^{(n)}t_R = \exp(-3n/4)$ with $n = 8, 9, \dots, 12$. The solid lines show $\rho(m|M)$ in the static limit where it is assumed that the TLSs do not switch during the measurement time $Mt_{\text{cyc}} = 3Mt_R$, with $M = 100$. Panels (a) and (b) refer to different coupling strengths. The color coding, which shows the values of M , is the same in the both panels.

III. THE CENTERED CORRELATOR AND THE VARIANCE

Convergence of a series of M measurement outcomes to the ergodic limit depends on how long there last correlations between the outcomes. An important characteristic

of the correlations is the centered pair correlator

$$\tilde{r}_2(k) = \left\langle (x_{n+k} - \langle x_{n+k} \rangle)(x_n - \langle x_n \rangle) \right\rangle \quad (2)$$

Here x_k is the outcome of k th measurement, $x_k \in \{0, 1\}$. A sequence of measurements approaches the ergodic limit only when its length M significantly exceeds the correlation length, i.e., $|\tilde{r}_2(M)/r_1| \ll 1$, where $r_1 \equiv \langle x_k \rangle$ is the average value of x_k . Generally, one may expect that the decay of $\tilde{r}_2(k)$ with the increasing k is an indicator of how fast the ergodicity is approached with the increasing number of measurements M .

For a periodic sequence of Ramsey measurements, the centered correlator $\tilde{r}_2(k)$ was calculated both for the case where the qubit frequency noise is due to the coupling to the TLSs and for the case where the noise is Gaussian [1]. In the case of coupling to TLSs, the general expression for $\tilde{r}_2(k)$ simplifies in the limit where $V^{(n)}t_R, W^{(n)}t_R \ll 1$. One can show that, in this limit, to the leading order in the small parameters,

$$\tilde{r}_2(k) \approx \frac{1}{4} e^{-2t_R/T_2} \sin^2 \phi_R \sum_n \left(w^{(n)} V^{(n)} t_R \right)^2 e^{-k W^{(n)} t_{\text{cyc}}},$$

$$w^{(n)} = 2(W_{01}^{(n)} W_{10}^{(n)})^{1/2} / W^{(n)}, \quad (3)$$

whereas

$$r_1 \equiv \langle x_k \rangle \approx \frac{1}{2} + \frac{1}{2} e^{-t_R/T_2} \cos \phi_R$$

$$\times \prod_n \left[1 - (w^{(n)} V^{(n)} t_R)^2 / 2 \right]; \quad (4)$$

the latter expression was used in the main text to give the position of the peak of $\rho(m|M)$ in the ergodic limit.

A peculiar feature of Eq. (3) is that $\tilde{r}_2(k)$ goes to zero for $\phi_R \rightarrow 0$. For small ϕ_R we need to take into account corrections of higher-order in $V^{(n)}t_R, W^{(n)}t_R$. Using the results [1] one can show that, for $\phi_R = 0$,

$$\tilde{r}_2(k) \approx \frac{1}{4} e^{-2t_R/T_2} \left\{ \sum_n \left[w^{(n)} V^{(n)2} (\Delta W^{(n)} / W^{(n)}) t_R^2 \right]^2 \right.$$

$$\times e^{-k W^{(n)} t_{\text{cyc}}} + \sum_{m_1=1}^{N_{\text{TLS}}} \sum_{m_2=1}^{m_1-1} \left(w^{(m_1)} w^{(m_2)} V^{(m_1)} V^{(m_2)} t_R^2 \right)^2$$

$$\left. \times \exp[-k(W^{(m_1)} + W^{(m_2)})t_{\text{cyc}}] \right\} \quad (5)$$

where $\Delta W^{(n)} = W_{10}^{(n)} - W_{01}^{(n)}$ is the difference of the switching rates of the n th TLS. As seen from Eq. (5), not only is $\tilde{r}_2(k)$ small for $\phi_R = 0$, but also, for symmetric TLSs, it falls off much more rapidly with the increasing k than for $\phi_R = \mathcal{O}(1)$.

Figure 4 shows $\tilde{r}_2(k)$ for the coupling to symmetric TLSs for the same parameters as in Fig. 2 of the main text. As seen from the left panel, $\tilde{r}_2(k)$ is smaller for 1 TLS than for 10 TLSs for the same $\phi_R = \pi/4$. But the most significant difference is between the results for 10 TLSs for $\phi_R = \pi/4$ and $\phi_R = 0$. This difference is

responsible for the difference by an order of magnitude in the values of M for which the ergodic limit is approached, as shown in the main text. It also leads to a very strong difference of the variances of the distribution shown in the right panel. The plot of σ_M^2 here is on the linear scale, in contrast to Fig. 2 of the main text. It shows approaching the ergodic limit in more detail.

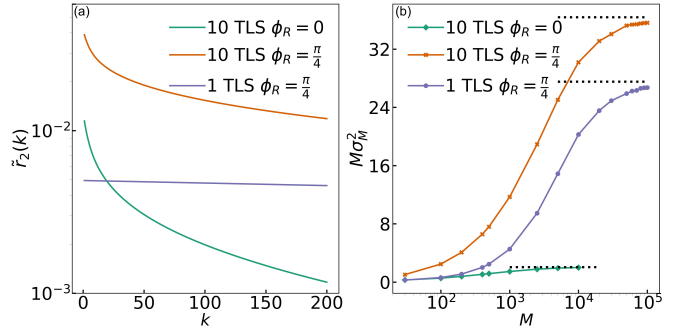


FIG. 4. Approaching the ergodic limit for noise from symmetric TLSs. Left panel: The calculated centered correlator $\tilde{r}_2(k)$ of the outcomes of qubit measurements for the qubit frequency noise from TLSs. The scaled coupling is $Vt_R = 0.2$. For a single symmetric TLS the scaled switching rate $Wt_R = 1.2 \times 10^{-4}$. For 10 symmetric TLSs the switching rates are $W^{(n)}t_R = \exp(-3n/4)$, $n = 3, 4, \dots, 12$. Right panel: calculated (solid lines) and simulated (dots) variance $\sigma_M^2 = \sum_m (m/M)^2 \rho(m|M) - r_1^2$ of the distribution of the outcome measurements. The dashed lines show the values of $M\sigma_M^2$ in the ergodic limit. The TLSs parameters are the same as in the left panel.

For qubit frequency fluctuations induced by weak Gaussian noise, we have, to the leading order,

$$\tilde{r}_2(k) \approx \frac{1}{4} e^{-2(t_R/T_2) - f_0} \left(f_k \sin^2 \phi_R + \frac{1}{2} f_k^2 \cos^2 \phi_R \right),$$

$$r_1 = \frac{1}{2} \left[1 + e^{-t_R/T_2} \exp(-f_0/2) \cos \phi_R \right],$$

$$f_k = \langle \theta_n \theta_{n+k} \rangle \quad (6)$$

(we do not expand $\exp(-f_0)$, as f_0 was not very small in the simulations shown in the main text). As seen from Eq. (6), for weak Gaussian noise $\tilde{r}_2(k)$ is much smaller for $\phi_R = 0$, similar to the case of weak noise from the TLSs.

In the main text, the analysis of Gaussian noise was done for $1/f$ -type noise with the parameters adjusted so as to make it similar to the noise from the 10 symmetric TLSs studied in the simulations with the same coupling constants, $V^{(n)} = V$ and $w^{(n)} = 1/4$. A comparison of the noises can be done by looking at their effect on the expectation value of the measurement outcome r_1 and the power spectra.

The power spectra $S_q(\omega)$ of the noise of the qubit frequency $\delta\omega_q(t)$,

$$S_q(\omega) = \int_{-\infty}^{\infty} dt e^{i\omega t} \langle \delta\omega_q(t) \delta\omega_q(0) \rangle,$$

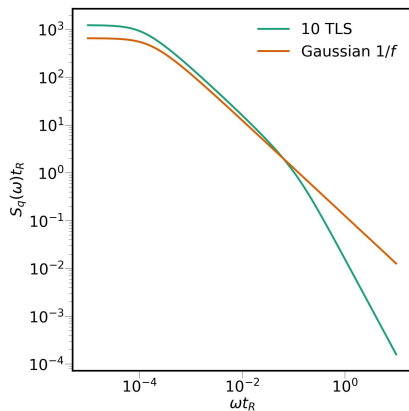


FIG. 5. Comparison of the power spectra of the $1/f$ -type Gaussian noise and the noise from 10 symmetric TLSs. Plotted are the scaled spectra $S_q^{\text{TLS}}(\omega)t_R$ and $S_q^{\text{Gauss}}(\omega)t_R$. The spectra are given by Eqs. (7) and (8). The spectra for TLSs refer to the system of 10 symmetric TLSs with the same parameters as those in Fig. 4. For the Gaussian noise we used $\omega_{\min} = \min W^{(n)}$, so that $\omega_{\min}t_R = \exp(-9) \approx 1.2 \times 10^{-4}$; $Dt_R = 0.1267$.

are shown in Fig. 5. For the noise from TLSs, the power spectrum has the form

$$S_q^{\text{TLS}}(\omega) = 2 \sum_{n=1}^{N_{\text{TLS}}} (w^{(n)}V^{(n)})^2 W^{(n)} / (W^{(n)2} + \omega^2), \quad (7)$$

whereas for the Gaussian noise we studied it has the form

$$S_q^{\text{Gauss}}(\omega) = \frac{2}{\pi} D_{\text{fl}} \int_{\omega_{\min}}^{\infty} \frac{dW}{W^2 + \omega^2} \quad (8)$$

As seen from Fig. 5, the spectrum $S_q^{\text{Gauss}}(\omega)$ is of $1/f$ type, with the low-frequency offset ω_{\min} . We chose ω_{\min} to be equal to the minimal switching rate of the 10 symmetric TLSs we used in the simulations, $\omega_{\min} = \min W^{(n)}$.

It is easy to see that, for $\omega_{\min}t_R \ll 1$, the parameter

f_0 that determines r_1 is

$$f_0 \approx (Dt_R^2/\pi)(3/2 - \gamma_E + |\log(\omega_{\min}t_R)|).$$

The value of f_0 that gives the same r_1 as the studied 10 symmetric TLSs was $f_0 \approx 0.4$. This value was used to determine the noise intensity D .

It is seen from Fig. 5 that the spectra of the TLS and Gaussian noise are close at low frequencies and show $1/f$ -scaling in a broad frequency range. This is why the distributions $\rho(m|M)$ for these noises in Fig. 2 of the main text were somewhat similar. Still, there was a significant difference between the distributions, which is important for identifying the source of the noise.

IV. INDEPENDENT MEASUREMENTS

It is instructive to compare the results on the distribution $\rho(m|M)$ with what is learned from independent Ramsey measurements separated by a time interval that largely exceeds the noise correlation time. Each such measurement has the probability

$$p[\theta(\ell)] = \frac{1}{2} \left[1 + \exp(-t_R/T_2) \cos(\theta(\ell) + \phi_R) \right]$$

to give “one” as an outcome. Here, the values of the phase $\theta(\ell)$ are random, they are enumerated by $\ell = 1, \dots, L$.

As the measurements are repeated, we may expect to obtain a binomial distribution of the outcomes. For the generating function of the distribution of the outcomes x_k of independent individual measurements we have

$$\begin{aligned} \left\langle \exp \left[(t/M) \sum_{k=1}^M x_k \right] \right\rangle &= \prod_k \left\langle \exp (tx_k/M) \right\rangle \\ &= \{1 + r_1 [\exp(t/M) - 1]\}^M, \end{aligned} \quad (9)$$

where $r_1 \equiv \langle x_k \rangle$ is the expectation value of x_k .

On the other hand, for the binomial distribution $\rho_{\text{binom}}(m|M)$, Eq. (3) of the main text, we have $\langle \exp(tm/M) \rangle = \{1 + r_1 [\exp(t/M) - 1]\}^M$. This expression coincides with the generating function (9).

[1] F. Wudarski, Y. Zhang, A. Korotkov, A. G. Petukhov, and M. I. Dykman, “Characterizing low-frequency qubit noise,” (2022), [arxiv:arXiv:2207.01740](https://arxiv.org/abs/2207.01740).